Computer Modeling in Engineering & Sciences
DOI:xxxxx
Type: XXXX

Tech Science Press

Meshless computational strategy for higher order strain gradient plate models

Francesco Fabbrocino[1], Serena Saitta[1] , Riccardo Vescovini[2], Nicholas Fantuzzi[3,*] and Raimondo Luciano[4]

[1]Telematic University Pegaso, Centro Direzionale Isola F2, Napoli, 80143, Italy.
[2]Politecnico di Milano, Via La Masa, 34, 20156, Milano, Italy.
[3]University of Bologna, Viale del Risorgimento 2, Bologna 40136, Italy.
[4]Parthenope University, Centro Direzionale ISOLA C4, 80133 Napoli, Italy.
[*]Corresponding Author: Nicholas Fantuzzi. Email: nicholas.fantuzzi@unibo.it.
Received: XXXX; Accepted: XXXX.

Abstract: The present research focuses on the use of a meshless method for the solution of nanoplates by considering strain gradient thin plate theory. Unlike the most common finite element method, meshless methods do not rely on a domain decomposition. In the present approach approximating polynomials at collocation nodes are obtained by using radial basis functions which depend on shape parameters. The selection of such parameters can strongly influences the accuracy of the numerical technique. Therefore the authors are presenting some numerical benchmarks which involve the solution of nanoplates by employing an optimization approach for the evaluation of the undetermined shape parameters. Stability is discussed as well as numerical reliability against solutions taken for the existing literature.

Keywords: meshless; strain gradient; nanoplates; radial basis functions

1 Introduction

In the broad context of meshless methods Meshless Local Petrov-Galerkin (MLPG) [1] demonstrated to have strong capabilities to solve problems where weakly-singular traction and displacement boundary integral equations are involved. Moreover, other problems in this context have been analyzed and solved [2, 3]. THe main idea of meshless methods is to go beyond the current limitations of finite element models for analyzing problems in mechanics [4]. Unlike classical FEM shape functions are developed for a scattered set of collocation nodes [4, 5] and their generation defines different meshless approaches. The one considered in the present work is named Radial Point Interpolation Method (RPIM) [6, 7, 8, 9] which has the fundamental property of Kronecker delta function [10, 11, 12, 13]. This approach makes the RPIM extremely easy to be implemented and used for the solution of any problem in structural mechanics.

It has been demonstrated to be extremely relevant in industrial applications for nanoengineering that nanoelectromechanical (NEMS) systems have been widely considered in the recent literature with several gradient elasticity problems [14, 15]. It has been demonstrated in recent literature that nano-structures are used for micro-sized systems and devices such as biosensors, nano-actuators and nano-electro-mechanical systems [16].

Among the vast literature of nonlocal theories stress-driven models have been recently presented for nanobeams presenting analytical solutions. For instance closed-form solution of Bernoulli and Timoshenko type for Erigen-like formulations and stress field and a bi-exponential averaging kernel functions characterized by a scale parameter is presented in [17, 18, 19]. Nonlocal strain gradient Bernoulli like beam models by considering special bi-exponential averaging kernels and functionally graded materials has been presented in [20]. Nonlocal beam formulations have been presented within a thermodynamic framework, variational formulation within its analytical solution has been provided in [21]. Nanobeams can be subjected to axial loads which leads to buckling, such effects must be considered for a proper nanoengineering design, thus stress-driven buckling of nanobeams can be found in [22, 23]. In the context of dynamic problems vibrations in nonlocal integral elasticity has been recently considered for beams and plates in [24, 25].

Most of the nonlocal theories relies on homogenization approaches which aim at simplifying the problem by considering less modelling parameters in composite materials [26, 27]. It is remarked that size effects and microstructures paved the way in presenting innovative and multiscale approches in solid mechanics [28, 29].

It has been demonstrated by several researchers that higher-order elasticity is becoming of paramount importance for solid mechanics as mentioned in [30, 31, 32]. In most researchers the term nonlocality has been brought by Eringen [33] and by Eringen and Edelen [34] where it can be found that the constitutive relations have to be modified to take into account their dependency on the mechanical properties of the entire body and not only of the properties in the neighbourhood of the material point. In this regard, in the present work nonlocal effects have be meaning introduced by by Altan and Aifantis [35, 36], which considered a simplified nonlocal model where all nonlocalities are concentrated in a gradient model similar to the one proposed by Mindlin [37]. Such approach, known as strain gradient theory, has been utilized also by others in other contexts in solid mechanics [38, 39, 40]. Strain gradient theory [41] has been demonstrated to be a constrained version of other higher-order unconstrained versions available in the literature such as couple stress [42, 43, 44] as well as micropolar theories [45, 46, 47].

In the framework of plate theories thin plate model is very common within the area of structural mechanics of investigating thin-walled structures [48, 49]. Such approach can be easily extended in order to consider composite structures such as laminated [50, 51] or sandwich ones [52].

In the present work the advantages of meshless methods are considered in the framework of strain gradient composite thin plate theory to solve such numerical problem.

2 Theoretical background

The present work considers the problem of laminated thin plates of rectangular plane form of size $a \times b$, where a, b indicate lengths with respect to x, y, respectively. The plate thickness is indicated with h and the plate represents the middle plane of the actual plate with z axis pointed normal to the x, y plate. Each ply which constitutes the stacking sequence is indicated with h_k and the total thickness is computed as $h = \sum_{k=1}^{N_L} h_k$, where N_L denotes the number of plies [53].

The present displacement field follows the classical thin plate theory and Cartesian displacements can be represented as [54]

$$\mathbf{U} = \mathbf{u} - z\mathbb{D}^{(s)}\mathbf{u}, \tag{1}$$

where $\mathbf{u}$ is the vector collecting the three middle plane displacements of the material point and $\mathbb{D}^{(s)}$ is the derivative operation defined in [55]. The strain vector ε is given by

$$\varepsilon = \varepsilon^{(m)} + z\varepsilon^{(b)}, \tag{2}$$

in which $\varepsilon^{(m)}$ and $\varepsilon^{(b)}$ denote respectively the membrane and bending strains, respectively. They can be evaluated as follows

$$\varepsilon^{(m)} = \mathbb{D}^{(m)}\mathbf{u}, \quad \varepsilon^{(b)} = \mathbb{D}^{(b)}\mathbf{u} \tag{3}$$

where the meaning of the differential operators $\mathbb{D}^{(m)}$, $\mathbb{D}^{(b)}$ is reported in [55] and [54].

BCs	$x=0,a$	$y=0,b$
Supported	$v=w=\frac{\partial w}{\partial y}=0$	$u=w=\frac{\partial w}{\partial x}=0$
Clamped	$u=v=w=\frac{\partial w}{\partial x}=\frac{\partial w}{\partial y}=0$	$u=v=w=\frac{\partial w}{\partial x}=\frac{\partial w}{\partial y}=0$
Free	No variables involved	No variables involved

Table 1: Essential boundary conditions considered.

Linear constitutive law is considered within the strain gradient theory as suggested in [40] allows to relate the membrane stresses in the k-th layer $\boldsymbol{\sigma}^{(k)}$ to the corresponding strain components ε as shown below [56, 57]

$$\boldsymbol{\sigma}^{(k)}=\left(1-\ell^2\nabla^2\right)\bar{\mathbf{Q}}^{(k)}\varepsilon, \tag{4}$$

in which the nonlocal parameter ℓ includes the micro/macro-scale interaction effects. The dependency of the stresses on the strain distribution within the medium is emphasized by the presence of the Laplacian in Cartesian coordinate system: $\nabla^2=\frac{\partial^2}{\partial x^2}+\frac{\partial^2}{\partial y^2}$. On the other hand, $\bar{\mathbf{Q}}^{(k)}$ represents the plane stress-reduced stiffness coefficients matrix of the k-th layer. The terms $\bar{Q}_{ij}^{(k)}$ of this matrix depend on the orthotropic properties of the layer (Young's moduli E_1, E_2, Poisson's ratio ν_{12} and shear modulus G_{12}), as well as by an arbitrary orientation $\theta^{(k)}$ as indicated in the book [58]. the $\mathbf{S}_N$ and $\mathbf{S}_M$ are the stress resultants that can be defined as follows

$$\begin{aligned}
\mathbf{S}_N&=\left(\mathbf{A}\mathbb{D}^{(m)}+\mathbf{B}\mathbb{D}^{(b)}-\ell^2\left(\mathbf{A}\mathbb{D}_{xx}^{(m)}+\mathbf{A}\mathbb{D}_{yy}^{(m)}+\mathbf{B}\mathbb{D}_{xx}^{(b)}+\mathbf{B}\mathbb{D}_{yy}^{(b)}\right)\right)\mathbf{u},\\
\mathbf{S}_M&=\left(\mathbf{B}\mathbb{D}^{(m)}+\mathbf{D}\mathbb{D}^{(b)}-\ell^2\left(\mathbf{B}\mathbb{D}_{xx}^{(m)}+\mathbf{B}\mathbb{D}_{yy}^{(m)}+\mathbf{D}\mathbb{D}_{xx}^{(b)}+\mathbf{D}\mathbb{D}_{yy}^{(b)}\right)\right)\mathbf{u},
\end{aligned}\tag{5}$$

The differential operators $\mathbb{D}_{xx}^{(m)}$, $\mathbb{D}_{yy}^{(m)}$, $\mathbb{D}_{xx}^{(b)}$, $\mathbb{D}_{yy}^{(b)}$ are defined in [54]. The constitutive operators $\mathbf{A}$, $\mathbf{B}$, $\mathbf{D}$ represent instead the membrane, membrane-bending coupling and bending stiffness matrices of the laminated composite plates [58].

In the current paper, isotropic and composite schemes are considered, therefore for some configurations $\mathbf{B}\neq\mathbf{0}$, thus, membrane and bending behaviors are coupled. The variational form of the present equilibrium is represented by [54, 59]

$$\begin{aligned}
0=\int_\Omega\Bigg\{&\left(\mathbb{D}^{(m)}\delta\mathbf{u}\right)^T\left(\mathbf{A}\mathbb{D}^{(m)}+\mathbf{B}\mathbb{D}^{(b)}\right)\mathbf{u}+\left(\mathbb{D}^{(b)}\delta\mathbf{u}\right)^T\left(\mathbf{B}\mathbb{D}^{(m)}+\mathbf{D}\mathbb{D}^{(b)}\right)\mathbf{u}\\
&+\ell^2\Bigg[\left(\mathbb{D}_x^{(m)}\delta\mathbf{u}\right)^T\left(\mathbf{A}\mathbb{D}_x^{(m)}+\mathbf{B}\mathbb{D}_x^{(b)}\right)\mathbf{u}+\left(\mathbb{D}_y^{(m)}\delta\mathbf{u}\right)^T\left(\mathbf{A}\mathbb{D}_y^{(m)}+\mathbf{B}\mathbb{D}_y^{(b)}\right)\mathbf{u}\\
&+\left(\mathbb{D}_x^{(b)}\delta\mathbf{u}\right)^T\left(\mathbf{B}\mathbb{D}_x^{(m)}+\mathbf{D}\mathbb{D}_x^{(b)}\right)\mathbf{u}+\left(\mathbb{D}_y^{(b)}\delta\mathbf{u}\right)^T\left(\mathbf{B}\mathbb{D}_y^{(m)}+\mathbf{D}\mathbb{D}_y^{(b)}\right)\mathbf{u}\Bigg]-\delta\mathbf{u}^T\mathbf{q}\,d\Omega,
\end{aligned}\tag{6}$$

The present meshless technique is applied to such variational statement of the problem.

3 Radial point interpolation method (RPIM)

In the present approach solution is obtained in scattered points located in the given plate rectangular domain. The approximating polynomials involved possess the Kronecker delta property which allows a straightforward implementation of boundary conditions. In the following implementation, in plane displacements u and v, transverse displacement w as well as rotations w_x, w_y are included in the numerical implementation even though more primary variables are involved in the present formulation [55, 54]. In the context of the strain gradient theory, the essential boundary conditions for the plate are shown in Table 1 where the four edges are identified by the values of the physical coordinates x and y.

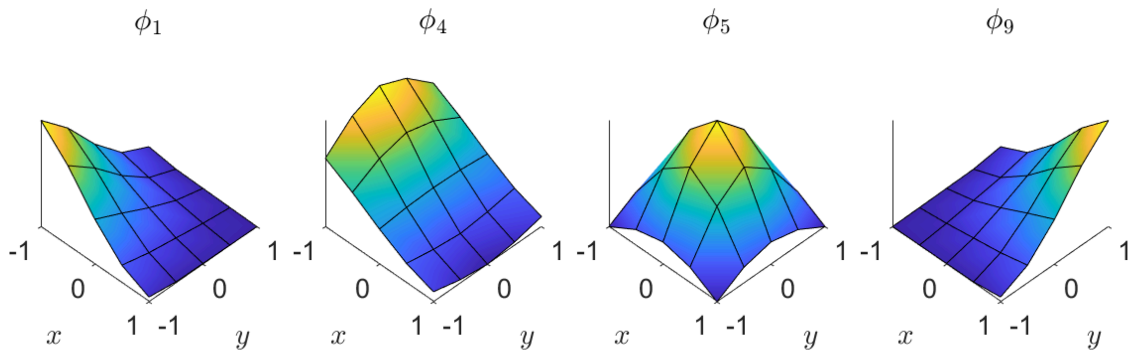

Figure 1: Sample of shape functions generation for a reference unitary domain.

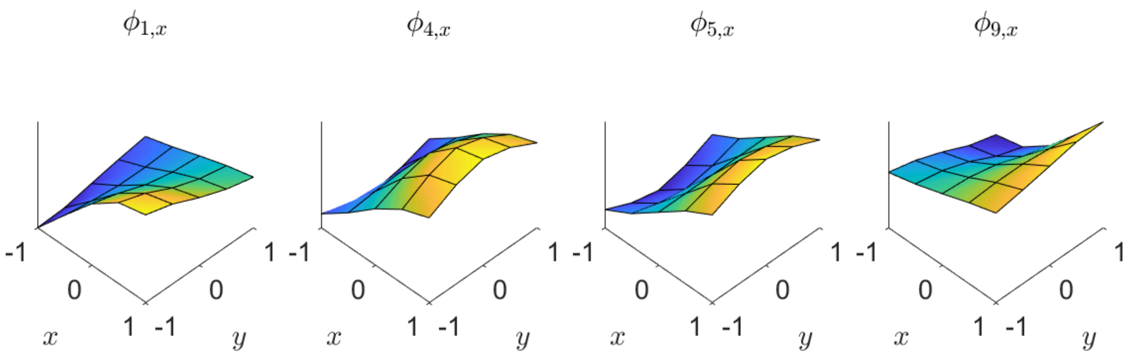

Figure 2: Shape functions of Figure 1 derived with respect to x.

Any other higher-order derivative is carried out by numerical derivation of the aforementioned parameters. Since both the deflection and its first derivatives are considered unknown, the Hermite-RPIM formulation is here presented. Let's consider a domain enclosing n arbitrarily scattered nodes. The approximation of the generic displacement $w(x,y)$ can be expressed as:

$$w(x,y) = \mathbf{R}^\top(\mathbf{x})\mathbf{a} + \mathbf{R}_{,x}^\top(\mathbf{x})\mathbf{a}^x + \mathbf{R}_{,y}^\top(\mathbf{x})\mathbf{a}^y \tag{7}$$

where $\mathbf{R}$, $\mathbf{R}_{,x}$ and $\mathbf{R}_{,y}$ are the vectors including the radial basis functions (RBF) and their derivatives. The correspondent coefficients are indicated using vectors $\mathbf{a}$, $\mathbf{a}^x$ and $\mathbf{a}^y$. For the following numerical applications the well-known multi-quadrics (MQ) RBF is used in its general form

$$R_i(x,y) = [(x-x_i)^2 + (y-y_i)^2 + C^2]^q \tag{8}$$

where $C = \alpha_C d_c$. Both q and α_C are shape parameters that have to be tuned while d_c is the average nodal spacing.

The vectors of coefficients in Equation (7) can be obtained by enforcing the field function and its derivatives to be satisfied at all the n nodes falling within the support domain of the point of interest (x,y). The support domain is a local domain, typically circular or rectangular, centered in a point of interest which can either be a node or an integration point. This leads to $3n$ linear equations

$$\mathbf{W} = \begin{bmatrix} \mathbf{R} & \mathbf{R}_{,x} & \mathbf{R}_{,y} \\ \mathbf{R}_{,x} & \mathbf{R}_{,xx} & \mathbf{R}_{,xy} \\ \mathbf{R}_{,y} & \mathbf{R}_{,xy} & \mathbf{R}_{,yy} \end{bmatrix} \begin{Bmatrix} \mathbf{a} \\ \mathbf{a}^x \\ \mathbf{a}^y \end{Bmatrix} = \mathbf{G} \begin{Bmatrix} \mathbf{a} \\ \mathbf{a}^x \\ \mathbf{a}^y \end{Bmatrix} \tag{9}$$

where $\mathbf{w}$, $\mathbf{w}_{,x}$ and $\mathbf{w}_{,y}$ are vectors of function values of the degrees of freedom considered in the collocation nodes. Thus, the independent parameter can be carried out as

$$w(x,y) = \left\{ \mathbf{R}^\top \quad \mathbf{R}_{,x}^\top \quad \mathbf{R}_{,y}^\top \right\} \mathbf{G}^{-1}\mathbf{W} = \mathbf{\Phi}^\top \mathbf{W} \tag{10}$$

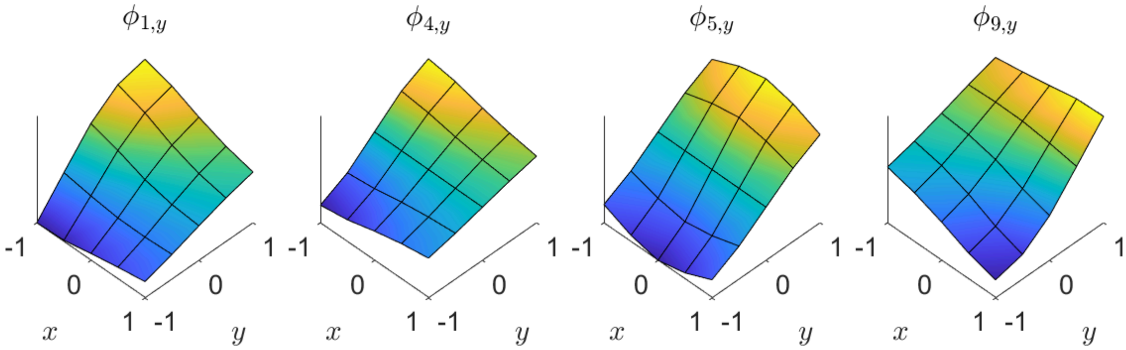

Figure 3: Shape functions of Figure 1 derived with respect to y.

An example of what the shape functions look like as computed with this method is given in Figure 1. A squared domain, represented by 3×3 regularly distributed nodes, is considered and all of the nodes are used to construct the shape functions for this domain. Figure 1 represents the shape functions and their first derivatives with respect to x and y for the nodes in the bottom left corner, in the middle left side, in the middle of the domain and in the top right corner respectively. For this particular case, the dimensionless parameters of the RBF are chosen as $C = 1$ and $q = 0.05$.

By following the same computational strategy of conventional finite element method [54] the algebraic form of the variational statement can be carried out because shape functions are evaluated at the collocation nodes. The needed integration is performed by following well-known Gauss integration rules. Solution of the present static problem is provided by Gauss elimination algorithm. The following section is dedicated to numerical results, stability and accuracy.

4 Applications

4.1 Isotropic plates

This section shows the results of the numerical analysis of isotropic Kirchhoff nanoplates modelled according to the second-order strain gradient theory and analysed by means of a mesh free RPIM. In this case, there is no coupling between the in plane and out of plane behaviour. Hence, the only unknown variables considered in the numerical implementation the are transverse displacement w and the rotations w_x, w_y The numerical codes are developed in MATLAB.

The results in terms of mid transverse displacement are presented in the nondimensional form as follows:

$$\bar{w} = \frac{1000wD}{q_z a^4} \tag{11}$$

where w is the central plate deflection, q_z is the magnitude of the transverse external load and D is the bending rigidity $D = Eh^3/12(1-\nu^2)$.

Nanoplates with different constraints are analysed, all having thickness $h = 0.34$ nm. Young's modulus and Poisson's ratio are taken as 1100 GPa and 0.3 respectively. Different nodal densities are also taken into account. Nanoplates represented by 3×3, 5×5, $7 \times\ 7$ and 11×11 equally spaced node grids are studied to analyse the convergence of the method. The local parameter ℓ also varies according to the analysis and results presented in the available literature [60].

The support domain used for the mesh free implementation has rectangular shape and is centered in the Gauss points. Its dimensions are considered in the classical way [4] $d_s = \alpha_s d_c$ where d_c is the average nodal spacing $d_c = \sqrt{\Delta x^2 + \Delta y^2}$ and α_s is a dimensionless parameter which, in this work, varies from 1.8 to 2.4.

Table 2: Values of $\bar{w}$ for 3×3 nodal distribution, obtained for $\alpha_C = 3$, $q = 1.3$, $\alpha_s = 2$.

BC	ℓ (nm)	Exact	Result	Error (%)
SSSS	0	4.0624	2.8622	29.5441
	0.2	4.0330	2.8338	29.7347
	0.5	3.8844	2.6956	30.6045
	1	3.4231	2.3142	32.3946
CCCC	0	1.2653	1.0716	15.3086
	0.2	1.2333	1.0555	14.4166
	0.5	1.0979	0.9785	10.8753
	1	0.7946	0.7762	2.3156
SCSC	0	1.9171	1.5481	19.2478
	0.2	1.8783	1.5269	18.7084
	0.5	1.7093	1.4247	16.6501
	1	1.3040	1.1519	11.6641
SFSF	0	15.0113	13.5089	10.0085
	0.2	14.9470	13.4511	10.0080
	0.5	14.6165	13.1711	9.8888
	1	13.5451	12.3957	8.4857
SCSF	0	11.2359	10.8262	3.6463
	0.2	11.1703	10.7635	3.6418
	0.5	10.8454	10.4568	3.5831
	1	9.8416	9.5731	2.7282

Note that, in this work, 2×2 Gauss integration points are used in each cell of the background integration mesh.

Results listed in Tables 2-5 compare the available analytical solutions [60] with the present ones in terms of percentage error:

$$err_{\%} = 100 \frac{|w_e - \bar{w}|}{w_e} \tag{12}$$

where w_e is the exact solution taken from the aforementioned references.

The provided comparison is performed for different boundary conditions, number of collocation nodes and nonlocal parameter values. The C and q coefficients characterising the MQ radial basis functions, as well as the nondimensional α_s support domain parameter, vary as the number of nodes changes.

In addition, a visualization of the deformed configuration of the nanoplates here analysed is shown in Figure 9.

4.2 Composite plates

A similar analysis is also performed on squared cross-ply laminates. Simply-supported (SSSS) laminates with lamination schemes 0, (0/90), $(0/90)_2$ and $(0/90)_4$, subjected to a sinusoidal load are analysed. The material property used are taken as $E_1/E_2 = 25$, $G_{12} = G_{13} = 0.5E_2$, $G_{23} = 0.2E_2$. Moreover, the thickness is given by $h = a/100$. As in the previous section, the results are compared in terms of nondimensional mid-deflection:

$$\bar{w} = w_0 \frac{E_2 h^3}{q_s a^4} \tag{13}$$

Table 3: Values of $\bar{w}$ for 5×5 nodal distribution, obtained for $\alpha_C = 2.38$, $q = 0.01$, $\alpha_s = 2.4$.

BC	ℓ (nm)	Exact	Result	Error $(\%)$
SSSS	0	4.0624	3.8549	5.1078
	0.2	4.0330	3.8262	5.1277
	0.5	3.8844	3.6844	5.1488
	1	3.4231	3.2736	4.3674
CCCC	0	1.2653	1.3058	3.2008
	0.2	1.2333	1.2774	3.5758
	0.5	1.0979	1.1466	4.4357
	1	0.7946	0.8384	5.5122
SCSC	0	1.9171	1.8851	1.6692
	0.2	1.8783	1.8509	1.4588
	0.5	1.7093	1.6903	1.1116
	1	1.3040	1.2914	0.9663
SFSF	0	15.0113	14.8721	0.9273
	0.2	14.9470	14.8087	0.9253
	0.5	14.6165	14.5144	0.6985
	1	13.5451	13.7290	1.3577
SCSF	0	11.2359	11.2265	0.0837
	0.2	11.1703	11.1623	0.0716
	0.5	10.8454	10.8529	0.0692
	1	9.8416	9.9527	1.1289

where q_s is the magnitude of the sinusoidal load, taken as 1. The analysis is performed using 11×11 regularly distributed nodes to represent the domain and 2×2 Gauss points to perform the numerical integration. The results of the analysis, compared in terms of percentage error as shown in Equation 12, are shown in Table 6.

5 Conclusions

In this work, strain gradient nanoplates, both isotropic and laminated, have been analyzed by means of the Radial Point Interpolation Method. The aim was to apply a RPIM formulation to thin plates modelled via strain gradient theory. Isotropic second order strain gradient Kirchhoff nanoplates with various boundary conditions are first analyzed. Numerical convergence with the analytical results achieved in recent literature was studied. In a similar way, cross-ply composite plates subjected to a sinusoidal load are also analysed. In this case, 11×11 nodes are used to represent the domain and different lamination sequences are considered. The paper provides a detailed explanation of the RPIM method theoretical and numerical implementation as well as theoretical notions in both explicit and matrix form. This work proves the validity of the RPIM for problems with higher order of derivatives involved.

Table 4: Values of $\bar{w}$ for 7×7 nodal distribution, obtained for $\alpha_C = 2.38$, $q = 0.01$, $\alpha_s = 2.4$.

BC	ℓ (nm)	Exact	Result	Error $(\%)$
SSSS	0	4.0624	3.9617	2.4788
	0.2	4.0330	3.9310	2.5291
	0.5	3.8844	3.7815	2.6491
	1	3.4231	3.3461	2.2494
CCCC	0	1.2653	1.2796	1.1302
	0.2	1.2333	1.2470	1.1108
	0.5	1.0979	1.1177	1.8034
	1	0.7946	0.8305	4.5180
SCSC	0	1.9171	1.9072	0.5164
	0.2	1.8783	1.8668	0.6123
	0.5	1.7093	1.7035	0.3393
	1	1.3040	1.3220	1.3804
SFSF	0	15.0113	14.9049	0.7088
	0.2	14.9470	14.8228	0.8309
	0.5	14.6165	14.5063	0.7539
	1	13.5451	13.7327	1.3850
SCSF	0	11.2359	11.2019	0.3026
	0.2	11.1703	11.1255	0.4011
	0.5	10.8454	10.8058	0.3651
	1	9.8416	9.9248	0.8454

Table 5: Values of $\bar{w}$ for 11×11 nodal distribution, obtained for $\alpha_C = 2$, $q = 1.4$, $\alpha_s = 2.3$.

BC	ℓ (nm)	Exact	Result	Error $(\%)$
SSSS	0	4.0624	4.0472	0.3742
	0.2	4.0330	4.0174	0.3868
	0.5	3.8844	3.8711	0.3424
	1	3.4231	3.4424	0.5638
CCCC	0	1.2653	1.2794	1.1144
	0.2	1.2333	1.2464	1.0622
	0.5	1.0979	1.1084	0.9564
	1	0.7946	0.8018	0.9061
SCSC	0	1.9171	1.9272	0.5268
	0.2	1.8783	1.8872	0.4738
	0.5	1.7093	1.7163	0.4095
	1	1.3040	1.3111	0.5445
SFSF	0	15.0113	11.2507	0.0566
	0.2	14.9470	11.1760	0.0214
	0.5	14.6165	10.8467	0.0089
	1	13.5451	9.9095	1.3761
SCSF	0	11.2359	11.2265	0.1317
	0.2	11.1703	11.1623	0.0510
	0.5	10.8454	10.8529	0.0120
	1	9.8416	9.9527	0.6899

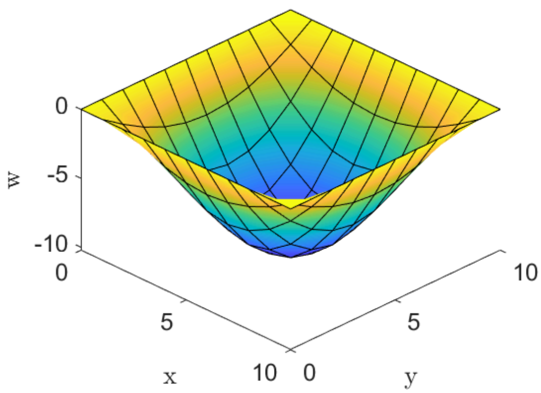

Figure 4: SSSS

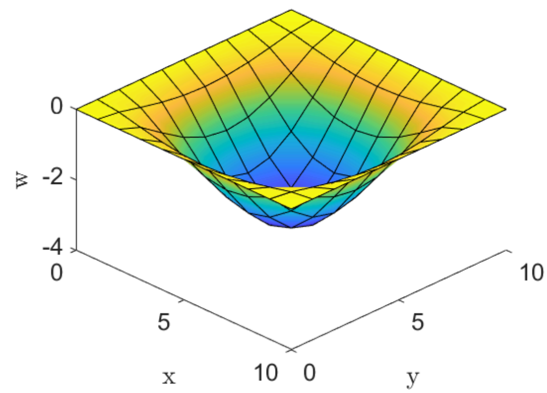

Figure 5: CCCC

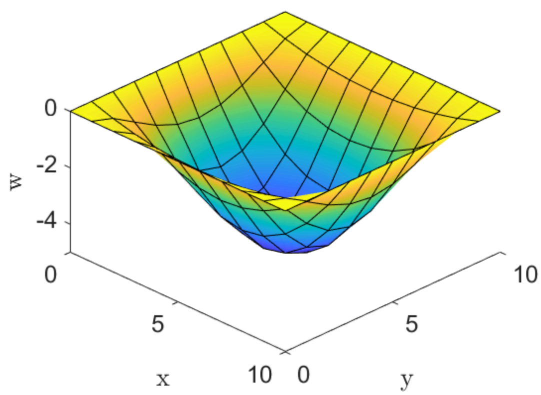

Figure 6: SCSC

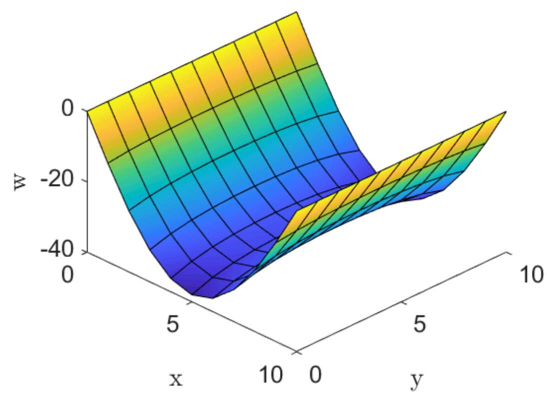

Figure 7: SFSF

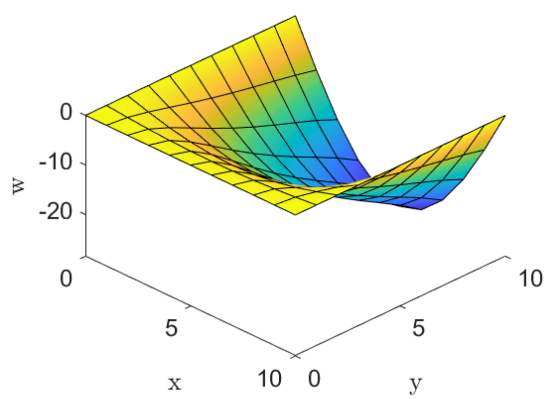

Figure 8: SCSF

Figure 9: Deformed shapes of square isotropic nanoplates with different boundary conditions.

Table 6: Non dimensional values of $\bar{w}$ mid deflection for composite nanoplates, obtained for $\alpha_C = 1.85$, $q = -1.6$, $\alpha_s = 2.4$.

ℓ (nm)	Laminate	Ref. [61]	Result	Error (%)
0	0	0.004312	0.004349	0.858071
	(0/90)	0.010636	0.010693	0.535916
	$(0/90)_2$	0.005065	0.005109	0.868707
	$(0/90)_4$	0.004479	0.004520	0.915383
0.05	0	0.002170	0.002137	1.520737
	(0/90)	0.003931	0.004033	2.594760
	$(0/90)_2$	0.002444	0.002351	3.805237
	$(0/90)_4$	0.002233	0.002167	2.955665
0.1	0	0.001450	0.001490	2.758621
	(0/90)	0.002522	0.002584	2.458366
	$(0/90)_2$	0.001623	0.001605	1.109057
	$(0/90)_4$	0.001490	0.001497	0.469799

Funding Statement: The authors received no specific funding for this study.

Conflicts of Interest: The authors declare that they have no conflicts of interest to report regarding the present study.

References

1. Atluri, S., Han, Z., Shen, S. (2003). Meshless local petrov-galerkin (MLPG) approaches for solving the weakly-singular traction & displacement boundary integral equations. *Computer Modeling in Engineering and Sciences*, *4*(*5*), 507–518.
2. Atluri, S. N., Zhu, T. (1998). A new meshless local petrov-galerkin (MLPG) approach in computational mechanics. *Computational Mechanics*, *22*(*2*), 117–127.
3. Atluri, S. N. (2004). *The Meshless Method (MLPG) for Domain & BIE Discretizations*, volume 677. Tech Science Press.
4. Liu, G. R. (2003). *Mesh Free Methods Moving beyond the Finite Element Method*. CRC Press LLC.
5. Liu, G., Gu, Y. (2005). *An Introduction to Meshfree Methods and Their Programming*. Springer Netherlands.
6. Xiangyang Cui, Guirong Liu, Guangyao Li (2011). A smoothed Hermite radial point interpolation method for thin plate analysis. *Arch. Appl. Mech.*, *81*, 1–18.
7. J. G. Wang, G. R. Liu (2002). A point interpolation meshless method based on radial basis functions. *Int. J. Numer. Meth. Engng.*, *54*, 1623–1648.
8. G. R. Liu, G. Y. Zhang, Y. T. Gu, Y. Y. Wang (2005). A meshfree radial point interpolation method (RPIM) for three-dimensional solids. *Comput. Mech.*, *36*, 421–430.
9. Yan Li, Guirong Liu, Zhiqiang Feng, Keishing Ng, Siuwai Li (2020). A node-based smoothed radial point interpolation method with linear strain fields for vibration analysis of solids. *Engineering Analysis with Boundary Elements*, *114*, 8–22.
10. Y. T. Gu, G. R. Liu (2001). A local point interpolation method for static and dynamic analysis of thin beams. *Comput. Methods Appl. Mech. Engrg.*, *190*, 5515–5528.
11. G. R. Liu, Y. T. Gu (2001). A point interpolation method for two-dimensional solids. *Int. J. Numer. Meth. Engng.*, *50*, 937–951.
12. G. R. Liu, X. Xu, G. Y. Zhang, Y. T. Gu (2009). An extended Galerkin weak form and a point interpolation method with continuous strain field and superconvergence using triangular mesh. *Comput. Mech.*, *43*, 651–673.
13. X. Xu, G. R. Liu, Y. T. Gu, G. Y. Zhang, J. W. Luo, J. X. Peng (2010). A point interpolation method with locally smoothed strain field (PIM-LS2) for mechanics problems using triangular mesh. *Finite Elements in Analysis and Design*, *46*, 862–874.
14. Tocci Monaco, G., Fantuzzi, N., Fabbrocino, F., Luciano, R. (2021). Critical temperatures for vibrations and buckling of magneto-electro-elastic nonlocal strain gradient plates. *Nanomaterials*, *11*(*1*), 87.
15. Tocci Monaco, G., Fantuzzi, N., Fabbrocino, F., Luciano, R. (2021). Trigonometric solution for the bending analysis of magneto-electro-elastic strain gradient nonlocal nanoplates in hygro-thermal environment. *Mathematics*, *9*(*5*), 567.
16. Chandel, V. S., Wang, G., Talha, M. (2020). Advances in modelling and analysis of nano structures: a review. *Nanotechnology Reviews*, *9*(*1*), 230 – 258.
17. Barretta, R., Fazelzadeh, S., Feo, L., Ghavanloo, E., Luciano, R. (2018). Nonlocal inflected nanobeams: A stress-driven approach of bi-helmholtz type. *Composite Structures*, *200*, 239–245.
18. Barretta, R., Caporale, A., Faghidian, S. A., Luciano, R., Marotti de Sciarra, F., et al. (2019). A stress-driven local-nonlocal mixture model for timoshenko nano-beams. *Composites Part B: Engineering*, *164*, 590–598.

19. Numanoglu, H., Ersoy, H., Civalek, O., Ferreira, A. (2021). Derivation of nonlocal fem formulation for thermo-elastic timoshenko beams on elastic matrix. *Composite Structures*, *273*, 114292.
20. Apuzzo, A., Barretta, R., Fabbrocino, F., Faghidian, S. A., Luciano, R., et al. (2019). Axial and torsional free vibrations of elastic nano-beams by stress-driven two-phase elasticity. *Journal of Applied and Computational Mechanics*, *5*(*2*), 402–413.
21. Ashida, F., Barretta, R., Luciano, R., Marotti de Sciarra, F. (2015). A fully gradient model for euler-bernoulli nanobeams. *Mathematical Problems in Engineering*, *2015*, 495095.
22. Barretta, R., Fabbrocino, F., Luciano, R., de Sciarra, F. M., Ruta, G. (2020). Buckling loads of nano-beams in stress-driven nonlocal elasticity. *Mechanics of Advanced Materials and Structures*, *27*(*11*), 869–875.
23. Civalek, Ö., Uzun, B., Yayli, M. Ö. (2021). Buckling analysis of nanobeams with deformable boundaries via doublet mechanics. *Archive of Applied Mechanics*, *91*(*12*), 4765–4782.
24. Apuzzo, A., Barretta, R., Faghidian, S., Luciano, R., Marotti de Sciarra, F. (2019). Nonlocal strain gradient exact solutions for functionally graded inflected nano-beams. *Composites Part B: Engineering*, *164*, 667–674.
25. Hadji, L., Avcar, M., Civalek, Ö. (2021). An analytical solution for the free vibration of fg nanoplates. *Journal of the Brazilian Society of Mechanical Sciences and Engineering*, *43*(*9*), 418.
26. Luciano, R., Barbero, E. J. (1995). Analytical Expressions for the Relaxation Moduli of Linear Viscoelastic Composites With Periodic Microstructure. *Journal of Applied Mechanics*, *62*(*3*), 786–793.
27. Luciano, R., Willis, J. (2005). Fe analysis of stress and strain fields in finite random composite bodies. *Journal of the Mechanics and Physics of Solids*, *53*(*7*), 1505–1522.
28. Trovalusci, P., Capecchi, D., Ruta, G. (2008). Genesis of the multiscale approach for materials with microstructure. *Archive of Applied Mechanics*, *79*(*11*), 981.
29. Mancusi, G., Fabbrocino, F., Feo, L., Fraternali, F. (2017). Size effect and dynamic properties of 2d lattice materials. *Composites Part B: Engineering*, *112*, 235–242.
30. Trovalusci, P., Augusti, G. (1998). A continuum model with microstructure for materials with flaws and inclusions. *J. Phys. IV France*, *08*, Pr8–383–Pr8–390. URL `https://doi.org/10.1051/jp4:1998847`.
31. Autuori, G., Cluni, F., Gusella, V., Pucci, P. (2017). Mathematical models for nonlocal elastic composite materials. *Advances in Nonlinear Analysis*, *6*(*4*), 355–382.
32. Gholami, Y., Ansari, R., Gholami, R. (2020). Three-dimensional nonlinear primary resonance of functionally graded rectangular small-scale plates based on strain gradeint elasticity theory. *Thin-Walled Structures*, *150*, 106681.
33. Eringen, A. C. (1972). Nonlocal polar elastic continua. *International journal of engineering science*, *10*(*1*), 1–16.
34. Eringen, A. C., Edelen, D. G. B. (1972). On nonlocal elasticity. *International journal of engineering science*, *10*(*3*), 233–248.
35. Altan, S., Aifantis, E. C. (1992). On the structure of the mode iii crack-tip in gradient elasticity. *Scripta Metallurgica et Materialia*, *26*(*2*), 319 – 324.
36. Altan, B. S., Aifantis, E. C. (1997). On some aspects in the special theory of gradient elasticity. *Journal of the Mechanical Behavior of Materials*, *8*(*3*), 231–282.
37. Mindlin, R. D. (1964). Microstructure in linear elasticity. *Archive for Rational Mechanics and Analysis*, *16*, 51–78.
38. Ru, C. Q., Aifantis, E. C. (1993). A simple approach to solve boundary-value problems in gradient elasticity. *Acta Mechanica*, *101*(*1*), 59–68.
39. Aifantis, E. C. (2003). Update on a class of gradient theories. *Mechanics of Materials*, *35*(*3*), 259 – 280.

40. Askes, H., Aifantis, E. C. (2011). Gradient elasticity in statics and dynamics: An overview of formulations, length scale identification procedures, finite element implementations and new results. *International Journal of Solids and Structures*, *48*(*13*), 1962 – 1990.
41. Eremeyev, V. A., Altenbach, H. (2015). *On the Direct Approach in the Theory of Second Gradient Plates*//H. Altenbach, G. I. Mikhasev. *Shell and Membrane Theories in Mechanics and Biology: From Macro- to Nanoscale Structures*. Cham: Springer International Publishing, 147–154.
42. Kim, J., Reddy, J. N. (2015). A general third-order theory of functionally graded plates with modified couple stress effect and the von kármán nonlinearity: theory and finite element analysis. *Acta Mechanica*, *226*(*9*), 2973–2998.
43. Ashoori, A., Mahmoodi, M. J. (2018). A nonlinear thick plate formulation based on the modified strain gradient theory. *Mechanics of Advanced Materials and Structures*, *25*(*10*), 813–819.
44. Żur, K. K., Arefi, M., Kim, J., Reddy, J. N. (2020). Free vibration and buckling analyses of magneto-electro-elastic fgm nanoplates based on nonlocal modified higher-order sinusoidal shear deformation theory. *Composites Part B: Engineering*, *182*, 107601.
45. Trovalusci, P. (2014). *Molecular Approaches for Multifield Continua: origins and current developments*//*Multiscale Modeling of Complex Materials: Phenomenological, Theoretical and Computational Aspects*. Vienna: Springer Vienna, 211–278.
46. Fantuzzi, N., Trovalusci, P., Dharasura, S. (2019). Mechanical behavior of anisotropic composite materials as micropolar continua. *Frontiers in Materials*, *6*, 59.
47. Tuna, M., Trovalusci, P. (2021). Stress distribution around an elliptic hole in a plate with âimplicitâ and âexplicitâ non-local models. *Composite Structures*, *256*, 113003.
48. Altenbach, H. (2000). On the determination of transverse shear stiffnesses of orthotropic plates. *Zeitschrift für angewandte Mathematik und Physik ZAMP*, *51*(*4*), 629–649.
49. Barretta, R., Luciano, R. (2015). Analogies between kirchhoff plates and functionally graded saint-venant beams under torsion. *Continuum Mechanics and Thermodynamics*, *27*(*3*), 499–505.
50. Bacciocchi, M., Tarantino, A. M. (2021). Third-order theory for the bending analysis of laminated thin and thick plates including the strain gradient effect. *Materials*, *14*(*7*), 1771.
51. Bacciocchi, M., Tarantino, A. M. (2021). Analytical solutions for vibrations and buckling analysis of laminated composite nanoplates based on third-order theory and strain gradient approach. *Composite Structures*, *272*, 114083.
52. Altenbach, H. (2000). An alternative determination of transverse shear stiffnesses for sandwich and laminated plates. *International Journal of Solids and Structures*, *37*(*25*), 3503 – 3520.
53. Cornacchia, F., Fabbrocino, F., Fantuzzi, N., Luciano, R., Penna, R. (2019). Analytical solution of cross- and angle-ply nano plates with strain gradient theory for linear vibrations and buckling. *Mechanics of Advanced Materials and Structures*, 1–15.
54. Bacciocchi, M., Fantuzzi, N., Luciano, R., Tarantino, A. M. (2021). Linear eigenvalue analysis of laminated thin plates including the strain gradient effect by means of conforming and nonconforming rectangular finite elements. *Computers & Structures*, *257*, 106676.
55. Bacciocchi, M., Fantuzzi, N., Ferreira, A. (2020). Conforming and nonconforming laminated finite element kirchhoff nanoplates in bending using strain gradient theory. *Computers & Structures*, *239*, 106322.
56. Tocci Monaco, G., Fantuzzi, N., Fabbrocino, F., Luciano, R. (2020). Hygro-thermal vibrations and buckling of laminated nanoplates via nonlocal strain gradient theory. *Composite Structures*, 113337.
57. Tocci Monaco, G., Fantuzzi, N., Fabbrocino, F., Luciano, R. (2021). Semi-analytical static analysis of nonlocal strain gradient laminated composite nanoplates in hygrothermal environment. *Journal of the Brazilian Society of Mechanical Sciences and Engineering*, *43*(*5*), 1–20.
58. Reddy, J. N. (2004). *Mechanics of Laminated Composite Plates and Shells: Theory and Analysis,*

Second Edition. CRC Press.
59. Bacciocchi, M., Fantuzzi, N., Ferreira, A. (2020). Static finite element analysis of thin laminated strain gradient nanoplates in hygro-thermal environment. *Continuum Mechanics and Thermodynamics*, 1–24.
60. Babu, B., Patel, B. (2019). Analytical solution for strain gradient elastic kirchhoff rectangular plates under transverse static loading. *European Journal of Mechanics - A/Solids*, *73*, 101–111.
61. Cornacchia, F., Fantuzzi, N., Luciano, R., Penna, R. (2019). Solution for cross- and angle-ply laminated kirchhoff nano plates in bending using strain gradient theory. *Composites Part B: Engineering*, *173*, 107006.